

PPPL- 5080

PPPL-5080

## Central Safety Factor and $B_N$ Control on NSTX-U via Beam Power and Plasma Boundary Shape Modification, using TRANSP for Closed Loop Simulations

M.D. Boyer, R. Andre, D.A. Gates, S. Gerhardt,  
I.R. Goumiri, J. Menard

November 2014



# Princeton Plasma Physics Laboratory

## Report Disclaimers

---

### Full Legal Disclaimer

This report was prepared as an account of work sponsored by an agency of the United States Government. Neither the United States Government nor any agency thereof, nor any of their employees, nor any of their contractors, subcontractors or their employees, makes any warranty, express or implied, or assumes any legal liability or responsibility for the accuracy, completeness, or any third party's use or the results of such use of any information, apparatus, product, or process disclosed, or represents that its use would not infringe privately owned rights. Reference herein to any specific commercial product, process, or service by trade name, trademark, manufacturer, or otherwise, does not necessarily constitute or imply its endorsement, recommendation, or favoring by the United States Government or any agency thereof or its contractors or subcontractors. The views and opinions of authors expressed herein do not necessarily state or reflect those of the United States Government or any agency thereof.

### Trademark Disclaimer

Reference herein to any specific commercial product, process, or service by trade name, trademark, manufacturer, or otherwise, does not necessarily constitute or imply its endorsement, recommendation, or favoring by the United States Government or any agency thereof or its contractors or subcontractors.

---

## PPPL Report Availability

### Princeton Plasma Physics Laboratory:

<http://www.pppl.gov/techreports.cfm>

### Office of Scientific and Technical Information (OSTI):

<http://www.osti.gov/scitech/>

---

### Related Links:

[U.S. Department of Energy](#)

[Office of Scientific and Technical Information](#)

# Central safety factor and $\beta_N$ control on NSTX-U via beam power and plasma boundary shape modification, using TRANSP for closed loop simulations

M. D. Boyer<sup>1</sup>, R. Andre<sup>1</sup>, D. A. Gates<sup>1</sup>, S. Gerhardt<sup>1</sup>, I. R. Goumiri<sup>2</sup>, J. Menard<sup>1</sup>

<sup>1</sup>Princeton Plasma Physics Laboratory, Princeton, New Jersey 08544, USA

<sup>2</sup>Department of Mechanical and Aerospace Engineering, Princeton University, Princeton, New Jersey 08544, USA

E-mail: mboyer@pppl.gov

August 2014

**Abstract.** The high-performance operational goals of NSTX-U will require development of advanced feedback control algorithms, including control of  $\beta_N$  and the safety factor profile. In this work, a novel approach to simultaneously controlling  $\beta_N$  and the value of the safety factor on the magnetic axis,  $q_0$ , through manipulation of the plasma boundary shape and total beam power, is proposed. Simulations of the proposed scheme show promising results and motivate future experimental implementation and eventual integration into a more complex current profile control scheme planned to include actuation of individual beam powers, density, and loop voltage. As part of this work, a flexible framework for closed loop simulations within the high-fidelity code TRANSP was developed. The framework, used here to identify control-design-oriented models and to tune and test the proposed controller, exploits many of the predictive capabilities of TRANSP and provides a means for performing control calculations based on user-supplied data (controller matrices, target waveforms, etc.). The flexible framework should enable high-fidelity testing of a variety of control algorithms, thereby reducing the amount of expensive experimental time needed to implement new control algorithms on NSTX-U and other devices.

## 1. Introduction

The National Spherical Torus eXperiment Upgrade facility (NSTX-U) [1], has been designed to bridge the gap between present ST devices, like NSTX [2] or the Mega-Ampere Spherical Tokamak (MAST) [3], and the requirements of future facilities that will study plasma material interaction [4], nuclear components [5], and generation of fusion power [6]. NSTX-U aims to improve understanding of key issues, such as the scaling of electron transport with field and current [7, 8, 9, 10], fast particle physics [11, 12, 13, 14], and sustainment of non-inductive, high- $\beta$  scenarios [15, 16, 17, 18, 19, 20]. The primary components of the upgrade are the complete replacement of the ‘center

stack', (containing the inner-leg of the toroidal field (TF) coils, the Ohmic heating (OH) solenoid, and some divertor coils), and the addition of a second neutral beam injector, aimed more tangentially. The upgrade will increase the TF capability from 0.55T to 1.0T, the maximum plasma current from 1.3 MA to 2.0 MA, and significantly increase auxiliary heating power, neutral beam current drive, and the ability to tailor their deposition profiles.

In order to achieve the goals of the NSTX-U program, advancements in plasma control will be essential, and work is underway to upgrade the hardware and software of the plasma control system (PCS) [21], and to develop the new control algorithms needed to optimally handle the complex dynamics of the system. The development of algorithms for plasma boundary shape control, power and particles exhaust control, current and rotation profiles control, and edge transport barrier control is in progress, and these efforts will build on the successful advances made on NSTX [22, 23, 24, 25, 26].

Due to its effect on confinement, plasma stability, and non-inductively driven plasma current, control of the safety factor profile will be critical to the NSTX-U program goals. Much progress in controlling the current profile has recently been made on several machines, including DIII-D, JET, and JT-60U, especially in the area of model-based feedback control. By combining the poloidal magnetic flux diffusion equation with empirical correlations obtained from physical observations and experimental data from DIII-D for the electron temperature, plasma resistivity, and non-inductive current drive, a simplified nonlinear model describing the dynamic response of the current profile to induction, the auxiliary heating and current drive systems, and the line average density in L-mode discharges was obtained [27]. The control-oriented model was used to design feedback controllers using robust [28], optimal [29], and backstepping [30] control design approaches, and the feedback controllers were successfully tested in experiments in DIII-D. A similar approach is currently being developed for NSTX-U. Using an alternative, purely data-driven approach to modeling, scenario-specific linear, dynamic, response models were recently obtained in JET [31], JT-60U, and DIII-D [32], which were used to design controllers for simultaneous control magnetic and kinetic plasma profiles.

In most studies of safety factor profile control, the plasma boundary shape is controlled (by a separate existing controller) at some constant reference, and the magnetic geometry is assumed to be fixed in time in the control design. However, modulation of the plasma shape has important effects on the bootstrap current, beam driven current deposition profiles, and magnetic flux diffusion, and therefore, the safety factor profile. Thus, plasma shape could serve as an additional degree of freedom in controller designs. While there are many shaping parameters that could be modified, there are several goals and constraints to consider when choosing a plasma boundary shape. On NSTX-U it is desirable to keep the inner plasma wall gap small to maintain low aspect ratio and best utilization of the TF. The upper and lower gaps should be kept small to achieve high elongation, and high plasma triangularity is needed to improve TF utilization. This leaves the outer-midplane plasma-wall gap as a free parameter

to manipulate for the purposes of safety factor profile control (though not considered in this work, the plasma ‘squareness’ could potentially be manipulated, provided the device has sufficient shaping flexibility [33, 34]). The outer-gap size is a trade-off, as a smaller outer-gap causes the plasma to fully fill the vessel, while a large outer gap increases elongation, and therefore bootstrap current. Increasing the outer gap size also causes the off-axis beams to drive current further off-axis. In [35], this trade-off was explored by generating a series of target plasma boundary shapes with identical X-point and inner-midplane radii, and identical X-point heights. Outer-gap sizes in the range of 5 to 20 cm were considered, with a corresponding range of elongation from 2.55 to 2.95 and aspect ratio from 1.71 to 1.81. It was observed that increasing the outer-gap size increased the central safety factor (and  $q_{min}$ ), which is critical for avoiding non-resonant  $m/n = 1/1$  kink modes [36, 37, 38, 20, 39], which are often coupled to 2/1 islands, on NSTX-U [40]. It was also seen that shine-through power becomes significant for large outer-gap, while the bad-orbit loss becomes significant for small outer-gap. The ideal-wall stability limit, resistive wall mode (RWM) stability, and vertical controllability will also depend on outer gap through varied coupling to the passive plates and elongation. The influence of the outer-gap on plasma parameters, combined with uncertainty in modeling, motivates the use of a feedback control system to alter the outer-gap size in response to real-time measurements of plasma performance.

In this work, we consider the controlled manipulation of the outer-midplane plasma-wall gap, along with the total beam power, as a potential means for controlling the central safety factor and  $\beta_N$  in NSTX-U. While this work focuses on just two actuators, the approach could later be integrated into a more complex profile control scheme that simultaneously modulates outer-gap size, beam power distribution, density, and loop voltage, providing an additional degree of freedom for achieving current profile targets. Two control design approaches were used, each using reduced models of the system dynamics. Since experimental data is not yet available for NSTX-U, these models were identified from simulated data generated using predictive TRANSP simulations (the proposed methods for identification can later be applied to experimental data). TRANSP, a time dependent code developed at Princeton Plasma Physics Laboratory for both prediction and analysis of tokamak experimental data [41, 42, 43], is one of the primary codes used in the fusion community. Several widely used modules, including NUBEAM [44] for calculating neutral beam heating and current drive, the ISOLVER free-boundary equilibrium solver [45, 46], are available for use within TRANSP and make it well suited for the predictive simulations required in this work.

Although the use of reduced models makes the control design process simpler, the highly coupled nonlinear nature of the tokamak can potentially lead to unexpected behavior when controllers tuned and tested on reduced models are experimentally tested. To minimize experimental time, a framework for conducting closed loop simulations of the proposed controller in TRANSP was developed. The framework makes use of many of the predictive capabilities of TRANSP mentioned above and includes a new module that enable the stored energy to be predicted based on confinement scaling expressions.

A means is provided for performing control calculations based on user-supplied data (controller matrices, target waveforms, etc.). Control calculations, performed based on user-supplied data (controller gain matrices, target waveforms, etc.) along with the acquisition of ‘real-time’ measurements and manipulation of TRANSP internal variables representing the control systems actuators, are implemented through a hook that allows custom run-specific code to be inserted into the standard TRANSP source code. The framework has the flexibility to simulate a variety of other control designs, and will enable fine-tuning of control laws, studies of robustness to scenario changes, studies of the impact of control laws on parameters not considered in the reduced models used for initial designs, and the demonstration of novel control schemes before devoting experimental time to their implementation. As shown in this work, integrated modeling simulations can also be used to generate control-oriented models based on simulated data to predict the effectiveness of system identification experiments and, in some cases, may remove the need for dedicated system identification experiments all together.

### 1.1. Organization

The paper is organized as follows. In Section 2, the computational approach used in the predictive TRANSP simulations is summarized and the modifications necessary for implementing closed loop control within TRANSP are introduced, while the implementation of these modifications is described in Section 3. The design and TRANSP simulation of the central safety factor and  $\beta_N$  control algorithms is presented in Section 4. Conclusions and future work are discussed in Section 5.

## 2. Overview of computational approach

The predictive TRANSP simulations in this work follow a similar approach to that used in the NSTX-U scenario development work done in [35]. In that work, the inputs to TRANSP were the time histories of the plasma boundary shape, total plasma current, electron temperature and density profiles, and the power, voltage, and geometry of the neutral beam injection. With these inputs, the TRANSP code was used to compute the solution to the poloidal-field equation [47], based on calculations of the bootstrap current, neutral beam current drive (NBCD), and free-boundary equilibrium. TRANSP was configured to compute the bootstrap current from the Sauter model [48] and the NUBEAM code [44] was used to compute the NBCD, with the beam-current shielding factor given by Lin-Liu and Hinton [49].

The free-boundary equilibrium was calculated using the ISOLVER equilibrium code within TRANSP [45, 46]. ISOLVER computes a free-boundary solution to the Grad-Shafranov equation that has boundary and X-point locations that best match a provided target plasma boundary. The target equilibria were generated using the stand-alone version of ISOLVER, based on the NSTX-U coil set. In an iterative procedure, a free-boundary equilibrium solution is obtained, the current and pressure profiles are

computed on the new equilibrium, and the equilibrium is recalculated.

In addition to equilibrium calculations, scenario studies require simulation of the ion and electron densities and thermal transport. Because experiments indicate that ion heat transport is reasonably well described by neoclassical theory [8, 9, 10, 50], the Chang-Hinton model [51] is used to model the ion temperature. However, because models for electron heat transport, external fueling, impurity sources, and particle transport are not as well validated, the evolutions of electron temperature and particle densities were not modeled by first-principles calculations.

To handle the unmodeled quantities, the following assumptions were made. First, the electron density profile was taken from an experimental profile measured on NSTX, scaled to achieve a particular Greenwald fraction  $f_{GW} = \bar{n}_e / (I_p / \pi a^2)$  [52, 53]. Assuming a flat  $Z_{eff} = 2$  profile, the ion density was calculated with carbon as the only impurity. The electron temperature was again taken from an experimental profile and scaled to achieve a particular global confinement level. The toroidal rotation profile was also taken from experiment and scaled inversely with the density. The scenario development simulations were run with experimental profiles from five different NSTX discharges to study the effect of profile shape on performance.

### *2.1. Modifications necessary for closed loop simulations*

The modeling approach described above was well-suited for scenario development work in which scans of different densities, temperatures, beam powers, and other parameters were done and the fully-relaxed profiles and performance indicators were compared. However, several modifications to the approach are necessary in order to develop a framework for closed loop simulations.

First, in the above approach, the temperature and density magnitudes were scanned until a particular confinement level and  $f_{GW}$  were achieved. This approach is not applicable in closed loop simulations, where it is necessary for the simulation to be constrained to follow a specified confinement level for all time, even as parameters like the plasma current and beam powers are varied, either by preprogrammed waveforms or based on the calculations of a feedback controller. This will ensure that, for example, the temperature used throughout the calculations in TRANSP increases appropriately if the total beam power is increased at the request of a control law. Depending on the nature of the control study, the density may also need to change in response to changes in parameters, either at the request of a feedback controller, or to ensure a particular  $f_{GW}$  or particle inventory is maintained throughout the simulation.

Secondly, although the inputs to TRANSP can be time-varying, the waveforms must be specified before initiating the run in the production version of TRANSP. For feedback control studies, it is necessary to update the input data throughout the simulation based on changing plasma parameters and the results of algorithm calculations. This requires both a means to modify TRANSP input data during the simulation and a way to include custom feedback control algorithms that calculate the new input data based on ‘real-

time' measurements of the plasma state. As the motivation for this work was testing current profile controllers, we have so far focused on enabling online modification of the density, beam powers, total plasma current, and plasma boundary, which are the most likely actuation methods for that particular problem. However, it is planned to extend this framework to enable modification of other parameters, for example the coil currents used by shape control algorithms.

### 3. Expert routine for feedback control simulations

The modifications necessary for closed loop simulations have been implemented through the so-called Expert routine. This routine is a hook, called at various places throughout the TRANSP source code, which can be used to insert run-specific custom code into the production version of TRANSP. A detailed description of the Expert routine developed for feedback control is provided in this section.

#### 3.1. Electron density specification

The electron density is taken to be of the form

$$n_e(\hat{\rho}, t) = n_{e,0}(t)n_e^{ref}(\hat{\rho}), \quad (1)$$

where  $n_e^{ref}$  is a user-supplied reference profile and  $n_{e,0}$  is a time-varying scale factor used to achieve continuity of the particle inventory  $N$ . The desired particle inventory,  $N^{req}$ , is either specified as a function of time or calculated to achieve a desired line-averaged density or Greenwald fraction. At the start of each TRANSP transport time step (covering the time interval  $(t_a, t_b)$ ), the desired inventory is calculated and the applied particle inventory is evolved using the equation

$$N_b = N_a + (t_b - t_a)(N^{req} - N_a)/\tau_N, \quad (2)$$

where  $\tau_N$  is an approximate density confinement time. For the simulations in this work,  $\tau_N = 0.1s$  (approximately a few multiples of the energy confinement time) was used. While this simplified model was suitable for this work, (2) could be replaced by a conservation equation that accounts for fueling sources and recycling.

For a particular inventory,  $N$ , the scale factor  $n_{e,0}$  is calculated from

$$n_{e,0} = \frac{N}{\int_0^1 n_e^{ref} \frac{\partial V}{\partial \hat{\rho}} d\hat{\rho}}. \quad (3)$$

Because TRANSP typically obtains the electron density from an input file, a call to the Expert routine must be made just after each time TRANSP accesses this input data. At each of these calls, the Expert file code interpolates the density profile for the appropriate time (TRANSP may look for density information at a time other than  $t_a$  or  $t_b$  during a particular transport step) and replaces the TRANSP internal variable for electron density with the calculated one.

### 3.2. Electron temperature specification and global confinement constraint

The electron temperature is taken to be of the form

$$T_e(\hat{\rho}, t) = T_{e,0}(t)T_e^{ref}(\hat{\rho}), \quad (4)$$

where  $T_e^{ref}$  is a user-defined reference profile and  $T_{e,0}$  is used to scale the temperature to maintain the stored energy predicted from a zero-dimensional (0D, volume averaged) energy balance. At the beginning of each transport step ( $t = t_a$ ), the value of the thermal stored energy  $W_{th}$  at the next step ( $t = t_b$ ) is calculated from the power balance (discretized using the Euler method)

$$W_{th,b} = W_{th,a} + (t_b - t_a) \left( -\frac{W_{th,a}}{\tau_E} + P_{net} \right), \quad (5)$$

where  $\tau_E$  is the confinement time and  $P_{net}$  is the net heating source calculated as the sum of all heating and loss terms from the thermal ion and electron power balance calculated by TRANSP. The confinement time is calculated based on one of two different assumptions. The first is the  $H_{98y,2}$  scaling expression [54], given by

$$\tau_{98y,2} = H_{98y,2} 0.0562 I_p^{0.93} B_T^{0.15} \bar{n}_e^{0.41} P_{Loss,th}^{-0.69} R_0^{1.97} \epsilon^{0.58} \kappa^{0.78}. \quad (6)$$

The second is a ST expression [7], given by

$$\tau_{ST} = H_{ST} 0.1178 I_p^{0.57} B_T^{1.08} \bar{n}_e^{0.44} P_{Loss,th}^{-0.73}. \quad (7)$$

In both expressions,  $I_p$  is the plasma current in MA,  $B_T$  is the toroidal magnetic field in T,  $\bar{n}_e$  is the line-averaged electron density in  $\#/m^3 \times 10^{19}$ ,  $R_0$  is the major radius in m,  $\epsilon$  is the inverse aspect ratio, and  $\kappa$  is the elongation. The loss power  $P_{Loss,th}$  is in MW and is defined in [7] as total input heating power less  $dW/dt$  and fast ion losses through charge-exchange, bad orbits, and shine-through. The factors  $H_{98y,2}$  or  $H_{ST}$  are interpolated from a user-supplied waveform.

Because TRANSP typically obtains the electron temperature from an input file, a call to the Expert routine is made just after each time TRANSP accesses the temperature input data. At each of these calls, the Expert file code interpolates the thermal stored energy  $W_{th}$  for the appropriate time based on  $W_{th,a}$  and  $W_{th,b}$ , the predicted values at  $t_a$  and  $t_b$  and calculates the required scale factor  $T_{e,0}$  for the reference profile. Noting that

$$E_{th} = \frac{3}{2} [n_e T_e + n_i T_i], \quad (8)$$

and using the volume average formula

$$\langle x \rangle = \frac{1}{V} \int_0^1 x \frac{\partial V}{\partial \hat{\rho}} d\hat{\rho}, \quad (9)$$

the volume averaged stored energy can be calculated as

$$\langle E_{th} \rangle = \frac{W_{th}}{V} = \frac{3}{2} [T_{e,0} \langle n_e T_e^{ref} \rangle + \langle n_i T_i \rangle]. \quad (10)$$

This can be solved for  $T_{e,0}$ , yielding

$$T_{e,0} = \frac{\frac{2}{3} \langle E_{th} \rangle - \langle n_i T_i \rangle}{\langle n_e T_e^{ref} \rangle}. \quad (11)$$

In these calculations, the  $n_i$ ,  $n_e$ , and  $T_i$  profiles are taken from the TRANSP internal variables at the current time step.

### 3.3. Equilibrium specification

The free-boundary equilibrium code ISOLVER can be operated in either ‘Circuit Equation Mode’, in which the coil currents are driven from input data, or in ‘Least Squares Mode’, in which the coil currents are calculated at each step to best fit a prescribed plasma boundary. While the former mode will be exploited in the future for testing feedback control algorithms for the shape, we have focused on using the latter operating mode in this work, i.e., we vary the target plasma boundary, but do not consider the design of the shape controller itself. Passive conducting structures, which will influence shape control through induced eddy currents, are not considered in this simulation mode, but will be included in future shape control studies using the ‘Circuit Equation Mode.’ At the start of each magnetic geometry calculation step, just after the inputs to ISOLVER are set up, the Expert routine is called and the existing plasma boundary reference and total plasma current value are replaced with the values requested by the control algorithm. In order to avoid crashes caused by these inputs varying too rapidly, the requests are first filtered with a low-pass filter with time constant  $\tau_G$  ( $\tau_G = 0.05s$  was used throughout the simulations in this work).

### 3.4. Control algorithm implementation

A flexible control algorithm has been implemented that allows testing of control laws that take the form of a discrete state-space system with a nonlinear transformation of the output. This algorithm was chosen because it accommodates many of the proposed current profile designs, but other custom algorithms can be implemented within the framework. The feedback control signal is calculated as the output of the system

$$\begin{aligned} x_c^{k+1} &= x_c^k + T (A_c x_c^k + B_c u_c^k), \\ y_c^k &= C_c x_c^k + D_c u_c^k, \end{aligned} \quad (12)$$

where  $A_c$ ,  $B_c$ ,  $C_c$ , and  $D_c$  are the user-specified controller system matrices,  $T$  is the user-specified sample time,  $x_c$  is the controller state,  $u_c$  is the input to the controller, and  $y_c$  is the output of the controller. The vector  $u_c$  is composed of the error measurements

$$u_c = y - y_{mod} - y_{tar}, \quad (13)$$

where  $y$  is the measured output,  $y_{mod}$  is the output modification signal from the anti-windup calculation (to be described) and  $y_{tar}$  is the corresponding set of targets. The vector  $y_c$  represents the feedback portion of the actuator requests,  $u$ , i.e.,

$$u_{fb} = y_c, \quad (14)$$

$$u_{ff} = u_r + u_{FFC} \quad (15)$$

$$u = u_{ff} + u_{fb} + u_{mod}. \quad (16)$$

The term  $u_{mod}$  is the actuator modification signal from the anti-windup calculation. The feedforward term  $u_{ff}$  is the combination of a user-specified set of actuator trajectories determined offline and an the result of calculations of an online feedforward compensator (to be used, for example, to account for measurable disturbances). A nonlinear transformation of the request  $u$  is applied to calculate the physical actuator requests  $v$ , i.e.,

$$v = f(u). \quad (17)$$

The default transformation is simply  $v = u$ , however, alternative transformations can be used to allow greater control design flexibility. We consider the presence of saturation limits on the actuators, and calculate

$$v_{sat} = sat(v), \quad (18)$$

$$u_{sat} = f^{-1}(v_{sat}), \quad (19)$$

where  $v_{sat}$  is the final actuator request, and we have applied the inverse of the transformation (17) to calculate the saturated controller request  $u_{sat}$ . The anti-windup signal is then calculated as the output of the system

$$\begin{aligned} x_{aw}^{k+1} &= x_{aw}^k + T \left( A_{aw} x_{aw}^k + B_{aw} u_{aw}^k \right), \\ y_{aw}^k &= C_{aw} x_{aw}^k + D_{aw} u_{aw}^k, \end{aligned} \quad (20)$$

where  $A_{aw}$ ,  $B_{aw}$ ,  $C_{aw}$ , and  $D_{aw}$  are the system matrices,  $x_{aw}$  is the state of the anti-windup system, and

$$u_{aw} = u - u_{sat}, \quad (21)$$

$$y_{aw} = [y_{mod}, u_{mod}]^T. \quad (22)$$

At the start of each transport time step in TRANSP (the shortest time scale in the simulation), the time since the last control calculation is compared with the desired controller sample time,  $T$ , to determine whether a control update should take place. Because the beam and geometry calculations are performed with longer step sizes than the transport calculations, and the inputs to these calculations cannot be updated at arbitrary times, control updates are aligned such that they take place just before the intervals at which these quantities are normally read in by TRANSP and the beam/geometry calculation step size is chosen to be a multiple of the controller sample time. The calculated actuator requests are saved and remain fixed until the next controller update, i.e., through several beam/geometry steps.

#### 4. Control of $q_0$ and $\beta_N$ with total beam power and outer gap size

In this section, the design and TRANSP testing of a novel  $q_0$  and  $\beta_N$  controller that uses the total beam power and outer gap of the plasma boundary as the manipulated variables is presented. To implement the outer-gap as an actuator in TRANSP, the stand-alone version of ISOLVER was used to generate two MHD equilibria: one with a gap size of 0.05m and the other with a gap size of 0.20m. The equilibria are compared

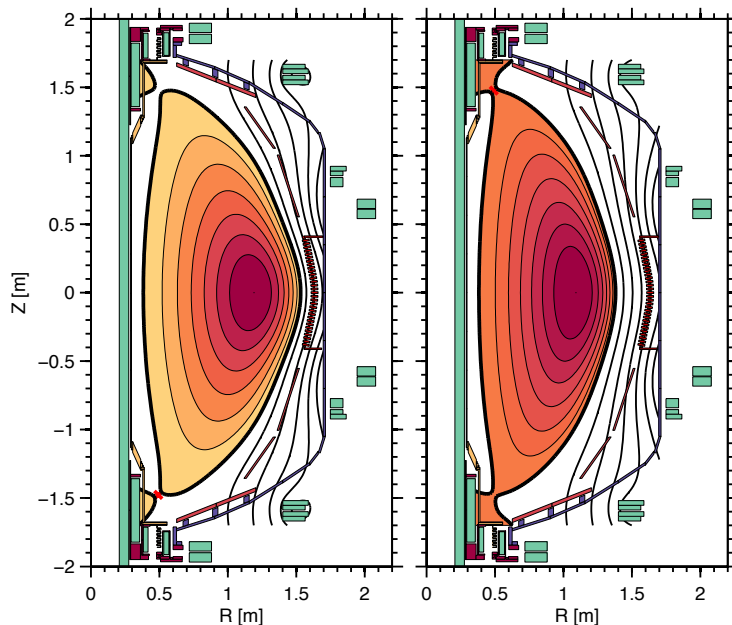


Figure 1: Cross-section of NSTX-U conducting structures comparing the two reference MHD equilibria with (left)  $g_{outer} = 0.05\text{m}$  and (right)  $g_{outer} = 0.20\text{m}$ .

in Figure 1. Given a requested outer-gap size, the Expert routine was programmed to calculate the target plasma boundary shape by interpolating between the plasma boundary shapes associated with these two reference equilibria. Two different design approaches are considered, a multi-input-multi-output (MIMO) controller and a design that splits the system into two single-input-single-output loops.

#### 4.1. Multi-input-multi-output design approach

In this section, the problem of controlling  $q_0$  and  $\beta_N$  using the total beam power and outer-gap-size is approached using modern control theory, which enables the constructive design of control laws for multi-input-multi-output systems. A system identification process was used to develop a linear state-space response model of the system, and this model was then used to design an optimal control law.

A linear state-space response model was sought of the form

$$\begin{aligned}\dot{\delta x} &= A\delta x + Bu_{fb}, \\ \delta y &= C\delta x + Du_{fb}.\end{aligned}\tag{23}$$

In this model, the physical actuator levels  $u = [P_{inj}, g_{outer}]^T$  are given by  $u = u_{ff} + u_{fb}$  where  $u_{ff}$  is a feedforward reference value and  $u_{fb}$  is the deviation from the reference. Similarly, the measurements of the system outputs  $y = [q_0, \beta_N]^T$  are given by  $y = y_{ff} + \delta y$ , where  $y_{ff}$  is the reference value associated with  $u_{ff}$  and  $\delta y$  is the deviation due to initial condition errors and the actuator deviation  $u_{fb}$ . In order to identify the system matrices  $A$ ,  $B$ ,  $C$ , and  $D$  for use in a model-based control design, a dedicated set of system identification experiments was conducted. First, a four second long simulation

(with  $I_p=0.6\text{MA}$ ,  $B_T = 1.0\text{T}$ ,  $N^{req} = 5.05 \times 10^{20}$ , and with  $n_e^{ref}$  and  $T_e^{ref}$  taken from NSTX shot 133964) was completed using the constant actuator values set at the mean of the actuator range ( $g_{outer} = 0.125\text{m}$ ,  $P_{inj} = 6.3\text{MW}$  distributed evenly among the six beam lines), representing  $u_{ff}$ . The steady-state value of  $q_0$  and  $\beta_N$  during this simulation was then taken to be  $y_{ff}$ . In the second simulation, the actuator values were modulated around  $u_{ff}$  in order to produce a deviation  $\delta y$ . In order to excite a range of frequencies for better identification of the model parameters, the modulation  $u_{fb}$  was chosen as a set of two pseudorandom binary sequences scaled by an amplitude  $A_{ID} = [2, 0.075]^T$ . The combined signal  $u = u_{ff} + u_{fb}$  used in the identification simulation is shown in Figure 2. The dataset  $(u_{fb}, \delta y)$  resulting from the 10s long simulation was then split into two intervals  $t_1 = (1.0, 6.0)\text{s}$  and  $t_2 = (6.0, 10.0)\text{s}$ , so that one set could be used for parameter estimation and the other could be used for model validation. The prediction error method [55] for state-space model identification, part of the Matlab System Identification Toolbox [56], was used to identify the optimal system matrices for a prescribed number of states  $n_x$  (model-order) that best matched the estimation data set. The optimal choice of model-order was then found by identifying a set of models for a small range of  $n_x$ , simulating the identified models using the inputs from the validation dataset, and comparing how well each model predicted the output of the validation dataset. Models with too few states fail to capture the dynamics of the system, while models with excessive states overfit the noise in the estimation data set, degrading prediction of the validation dataset. A comparison of the output of the optimal model, which was found to be of order four, to the validation data is shown in Figure 3, showing good agreement in  $q_0$  and excellent agreement in  $\beta_N$ .

The identified model was then used to design a linear-quadratic-Gaussian servo controller [57]. This type of controller minimizes a cost function of the form

$$J = E \left\{ \lim_{\tau \rightarrow \infty} \int_0^\tau \left( \begin{bmatrix} \delta x^T & u_{fb}^T \end{bmatrix} Q_{xu} \begin{bmatrix} \delta x \\ u_{fb} \end{bmatrix} + x_i^T Q_i x_i \right) dt \right\}, \quad (24)$$

where  $x_i$  is the integral of the tracking error, for a system of the form

$$\begin{aligned} \dot{\delta x} &= A\delta x + Bu_{fb} + w, \\ \delta y &= C\delta y + Du_{fb} + v, \end{aligned} \quad (25)$$

where the process noise  $w$  and measurement noise  $v$  are Gaussian white noise signals with covariance given by a matrix  $Q_{wv}$ . The controller optimizes the use of actuators according to the weights in  $Q_{xu}$ , which are free design parameters, and also ensures reference tracking with the ‘integral action’ tailored by choice of the free design parameters in  $Q_i$ . A Kalman filter is embedded in the resulting control law, which optimally estimates the unmeasured states  $\delta x$  based on the measurements  $\delta y$ , taking into account the process and measurement noise levels. The identified model was simulated using Simulink in order to tune the free design parameters to achieve a desired system response.

The controller was then tested in a TRANSP simulation using the proposed simulation framework (again with  $I_p=0.6\text{MA}$ ,  $B_T = 1.0T$ ,  $N^{req} = 5.05 \times 10^{20}$ , and with  $n_e^{ref}$  and  $T_e^{ref}$  taken from NSTX shot 133964). Time-dependent results of the closed loop simulation of the MIMO control law are shown in Figure 4. Figures 4(a) and (b) show the successful tracking of the time-varying targets for  $q_0$  and  $\beta_N$ . Neither  $q_0$  or  $\beta_N$  exhibit significant overshoot or oscillations (other than those caused by numerical noise). The beam-driven, bootstrap, and non-inductive current fractions are compared in Figure 4(c). While the bootstrap current increased at the second operating point, the beam-driven fraction decreased. There is therefore little change in the total non-inductive fraction. The response of the actuators  $g_{outer}$  and  $P_{inj}$  are shown in Figures 4(d) and (e), respectively. Note that the outer-gap request saturated after the step change in the target at  $t = 4.0\text{s}$ , but performance did not deteriorate significantly due to the presence of an anti-windup scheme. Finally, the density, shown in Figure 4(f), increased as the outer-gap-size was increased and the plasma volume decreased, since the particle inventory was held fixed during the simulation.

Profiles at the end of the two target steps are compared in Figure 5. The first operating point had a low  $q_0$  and the safety factor profile was monotonic as a result of low bootstrap current and beam-driven current peaked on-axis. At the second operating point, the bootstrap current increased slightly while the beam-driven current decreased on-axis (inside  $\hat{\rho} = 0.35$ ). The combination of these two effects made the total non-inductive current drive distribution peaked further off-axis, causing an increase in  $q_0$ . The safety factor profile became very slightly reverse shear. The coil currents needed to produce the requested plasma boundary shapes are depicted in Figure 6, showing that the expected currents are within physical limits and that the time-evolutions appears to be physically achievable, implying the proposed control approach should be experimentally feasible.

To study the robustness of the control law to changes in electron density and temperature profile shapes, the simulation was repeated with  $T_e^{ref}$  and  $n_e^{ref}$  taken from NSTX shot 121123 (instead of 133964 as in the system identification and first testing simulations). Results of this test are shown in Figure 7. A comparison of the reference electron temperature and density profiles used in the perturbed case (from 121123) and the design case (from 133964) is shown in Figures 7(a) and (b). The temperature profile is more narrow in the perturbed case, and the density profile exhibits a region with a reduced gradient. Figures 7(c) and (d) show that the controller performance is not significantly affected by the profile change (compare to the results shown in Figure 4). The  $q$  profiles achieved at the end of the simulations ( $t = 7.0\text{s}$ ) are compared in Figure 7(e), showing that although the controller forces  $q_0$  to match, the (uncontrolled) shape of the  $q$  profile differs. This change in shape can be attributed to the difference in the bootstrap current profiles, compared in Figure 7(f), that resulted from altering the electron temperature and density profile shapes.

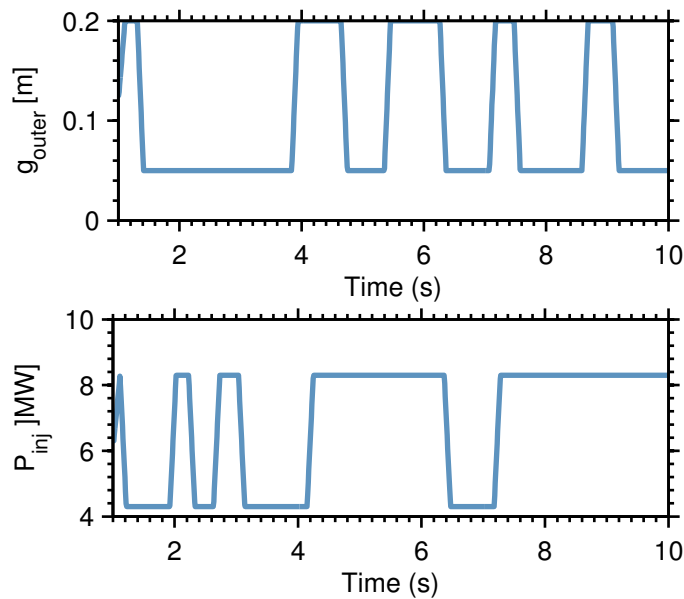


Figure 2: Actuator requests used in the system identification simulation.

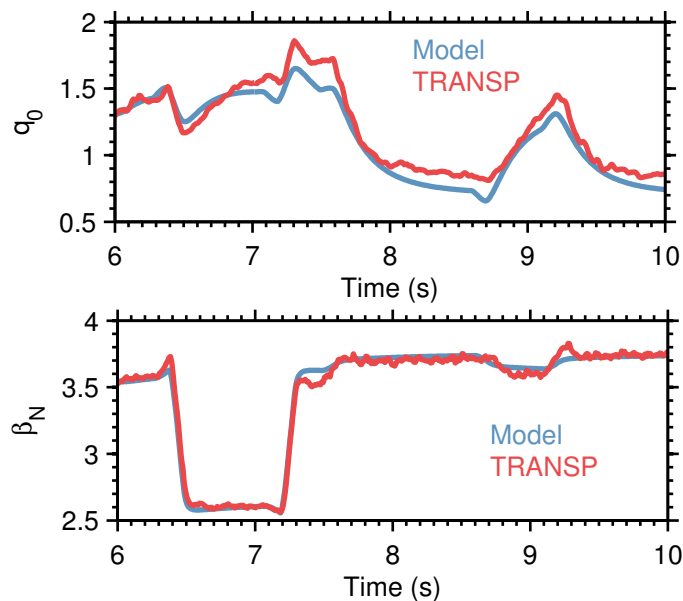


Figure 3: Comparison of output predicted by identified model to the actual output of the validation dataset.

#### 4.2. Two loop design approach

The results of the system identification simulation indicated that the response of  $\beta_N$  is dominated by the beam power and the response of  $q_0$  is highly dependent on  $g_{outer}$  (note in Figure 3, for example, that  $\beta_N$  remains approximately constant after  $t = 7.25$ s, despite modulation of  $g_{outer}$ ). This observation, along with the large timescale difference between the evolution of  $q_0$  and the evolution of  $\beta_N$ , suggests that a two-loop control structure may be appropriate. Although this approach neglects some of the coupling

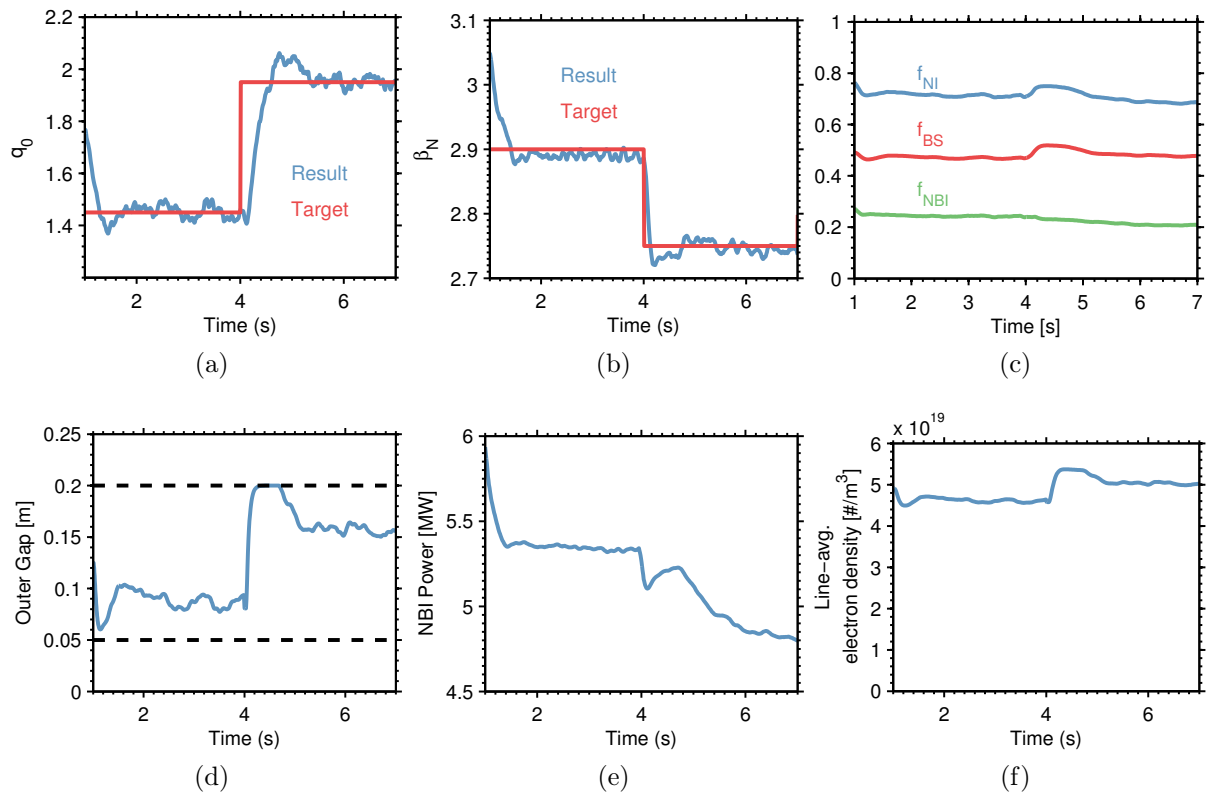


Figure 4: Results of closed loop simulation of the MIMO control law: (a)  $q_0$  result compared to target, (b)  $\beta_N$  compared to target, (c) non-inductive current fractions, (d) outer gap, (e) injected power, and (f) electron density.

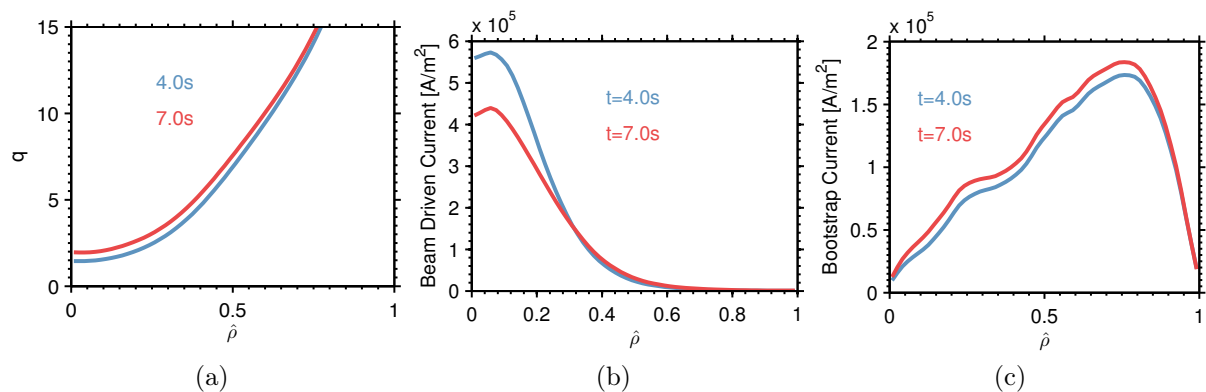


Figure 5: Results of closed loop simulation of the MIMO control law: (a)  $q$  profiles, (b) beam driven current profiles, and (c) bootstrap current profiles.

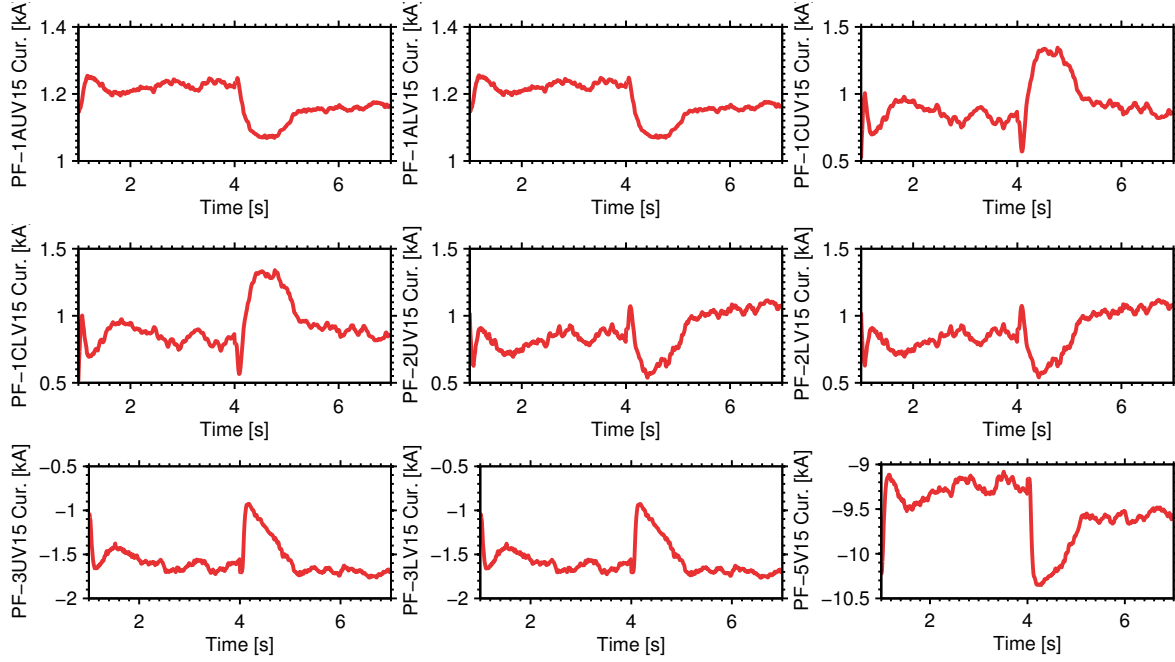


Figure 6: Poloidal field coil currents during closed loop simulation of the MIMO control law.

in the system, single-input-single-output control laws are more intuitive and easier to retune. The system identification procedure is also less involved than the previous case, which may be desirable if experimental time for control development is very limited (note that this point may be made irrelevant if it is found that system identification based on TRANSP predictive simulations alone is sufficient for control design). First, a controller for  $\beta_N$  using the total beam power as the manipulated variable was designed based on a simplified model of the stored energy dynamics. Next a controller for  $q_0$  using the outer gap as the manipulated variable was designed based on an identified approximate model for the central safety factor dynamics. PID controllers were designed for each of these single-input-single-output loops. A PID controller is a generic feedback control loop structure that calculates corrective action to minimize the error between a controlled variable and a desired set point by weighting the error, its integral over time, and its time derivative. This corrective action can be written as

$$u_{fb}(t) = K_P u_c(t) + K_I \int_0^t u_c(\tau) d\tau + K_D \frac{du_c(t)}{dt}. \quad (26)$$

The free gain parameters  $K_P$ ,  $K_I$ , and  $K_D$  for each loop were tuned based on approximate models of the dynamics of the system. For the  $\beta_N$  loop, noting that  $\beta_N = 100 \frac{\beta_T a B_T}{I_p}$ , where  $\beta_T = \frac{2\mu_0(2/3W)}{VB_T^2}$ , the dynamics were approximated by

$$\begin{aligned} \dot{\beta}_N = & \frac{400a\mu_0}{3I_p B_T V} \dot{W} + \frac{400\mu_0 W}{3I_p B_T V} \dot{a} - \frac{400a\mu_0 W}{3I_p B_T V^2} \dot{V} \\ & - \frac{400a\mu_0 W}{3I_p B_T^2 V} \dot{B}_T - \frac{400a\mu_0 W}{3I_p^2 B_T V} \dot{I}_p, \end{aligned}$$

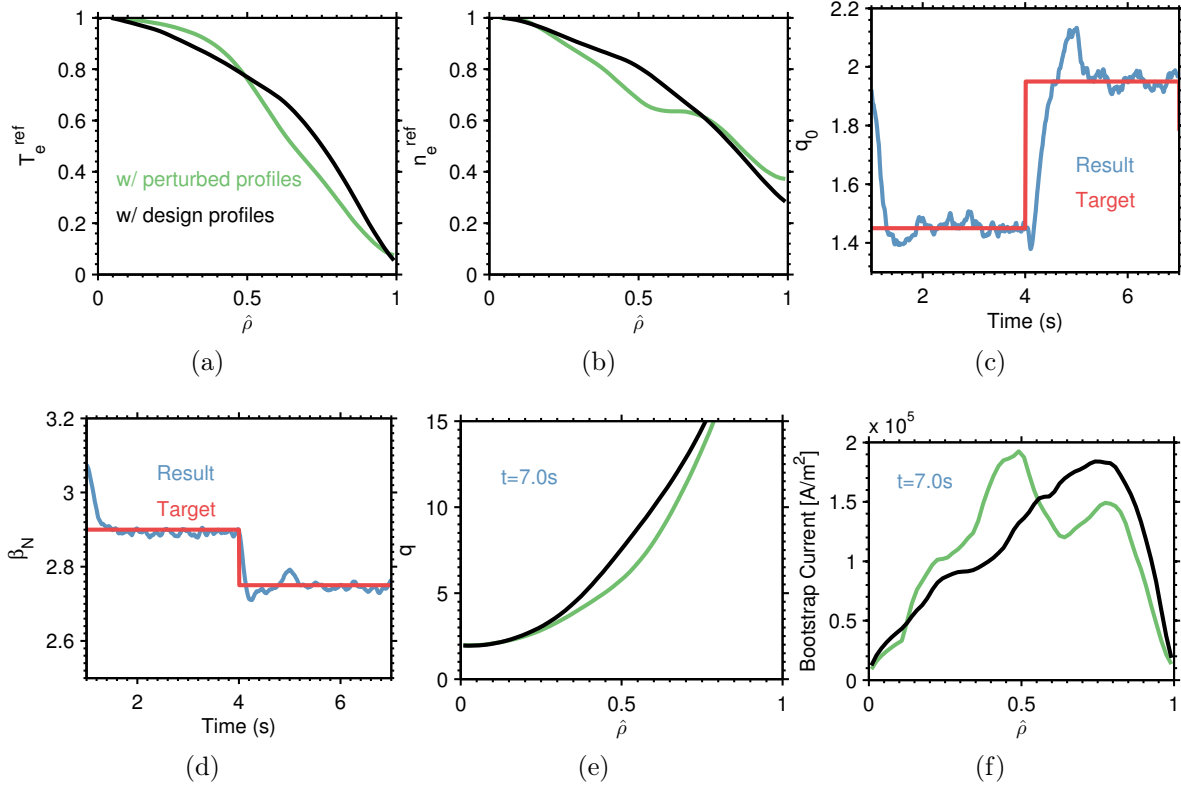


Figure 7: Results of closed loop simulation of the MIMO control law with modified reference profiles: (a) comparison of modified electron temperature reference profile to the one used for design, (b) comparison of modified and design electron density reference profiles, (c)  $q_0$  result compared to target, (d)  $\beta_N$  compared to target, (e) comparison of  $q$  profiles at  $t = 7.0s$  in each case, and (f) comparison of bootstrap current profiles at  $t = 7.0s$  in each case.

$$\begin{aligned}
&= \frac{400a\mu_0}{3I_p B_T V} \left( -\frac{W}{\tau_E} + P_{net} \right) + \frac{400\mu_0 W}{3I_p B_T V} \dot{a} \\
&\quad - \frac{400a\mu_0 W}{3I_p B_T V^2} \dot{V} - \frac{400a\mu_0 W}{3I_p B_T^2 V} \dot{B}_T - \frac{400a\mu_0 W}{3I_p^2 B_T V} \dot{I}_p.
\end{aligned} \tag{27}$$

We consider the heating to be dominated by the injected beam power, i.e.,  $P_{net} \approx P_{inj}$ , define  $u = \frac{400a\mu_0}{3I_p B_T V} P_{inj}$  as a virtual actuator, and lump the last four terms into a single disturbance term denoted by  $d$ , to write

$$\dot{\beta}_N = -\frac{\beta_N}{\tau_E} + u + d. \tag{28}$$

We consider a set of reference trajectories  $u_{ff}$  and  $d_{ff}$ , and the associated evolution of  $\beta_N$ , denoted  $\beta_{N,ff}$ , which is governed by

$$\dot{\beta}_{N,ff} = -\frac{\beta_{N,ff}}{\tau_{E,ff}} + u_{ff} + d_{ff}. \tag{29}$$

Denoting deviations of a signal  $z$  from its reference value as  $\delta z = z - z_{ff}$ , the dynamics of  $\delta\beta_N$  can be written as

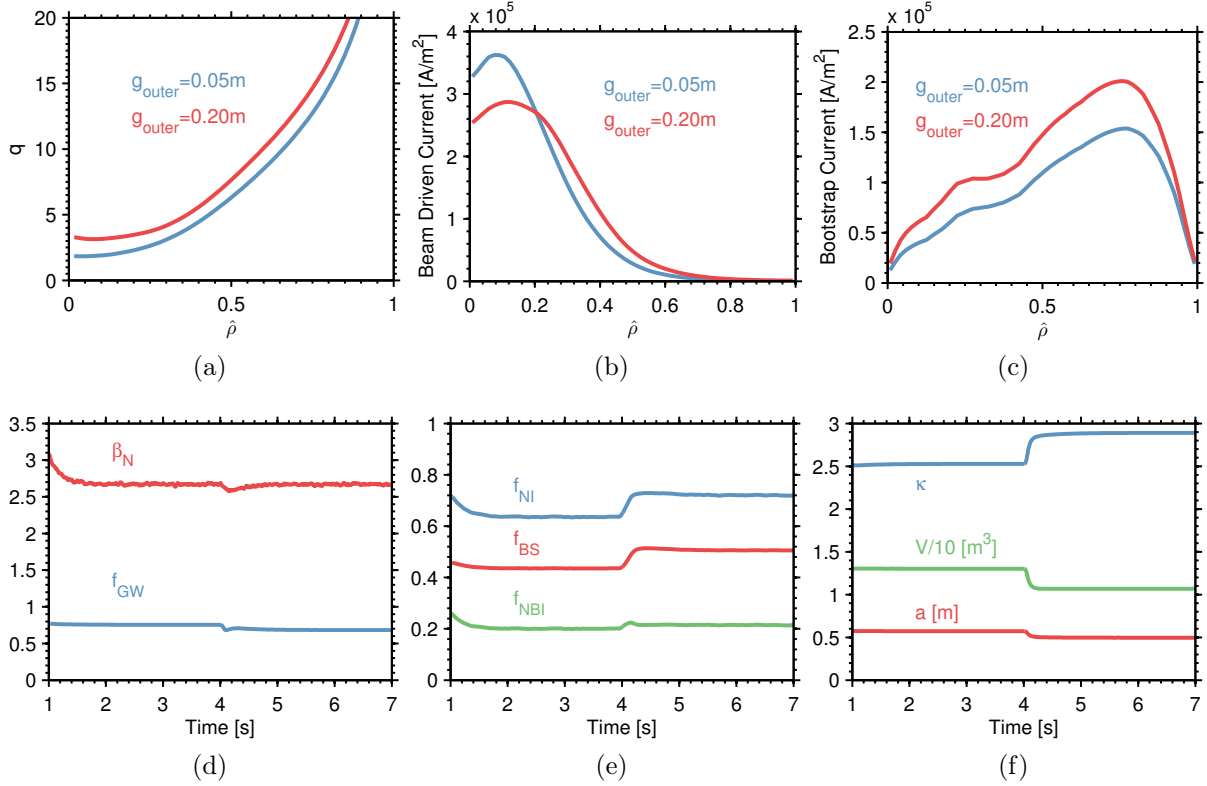


Figure 8: Results of open loop simulation used for system identification for the two-loop control scheme: (a)  $q$  profile, (b) beam driven current drive, (c) bootstrap current, (d)  $\beta_N$  and  $f_{GW}$ , (e) current fractions, and (f) shape related parameters.

$$\begin{aligned}\dot{\delta\beta}_N &= -\theta\beta_N + u + d + \theta_{ff}\beta_{N,ff} - u_{ff} - d_{ff} \\ &= -\theta\delta\beta_N - \delta\theta\beta_{N,ff} + \delta u + \delta d,\end{aligned}\quad (30)$$

where  $\theta = \frac{1}{\tau_E}$ . We choose the control law

$$\delta u = -\delta d + \delta\theta\beta_{N,ff} - K_{P,\beta}\delta\beta_N - K_{I,\beta}\int_0^t \delta\beta_N d\tau.\quad (31)$$

where  $K_{P,\beta} > 0$  and  $K_{I,\beta} > 0$ . The first two terms cancel the effect of disturbances, while the last two terms add proportional and integral feedback, increasing speed of response and ensuring disturbance rejection (and target tracking if  $\delta\beta_N$  is replaced by  $\beta_N - \beta_{N,r}$  in the control law, where  $\beta_{N,r}$  is the desired target). A PI controller was found to be sufficient for this design. The design parameters  $K_{P,\beta}$  and  $K_{I,\beta}$  were tuned to achieve a desirable response through Simulink simulations of the system.

The dynamics of  $q_0$  were modeled by a first-order-plus-dead-time (FOPDT) model, which can be written in the time-domain as

$$\dot{y}(t) = -\frac{y(t) + Ku(t-L)}{T},\quad (32)$$

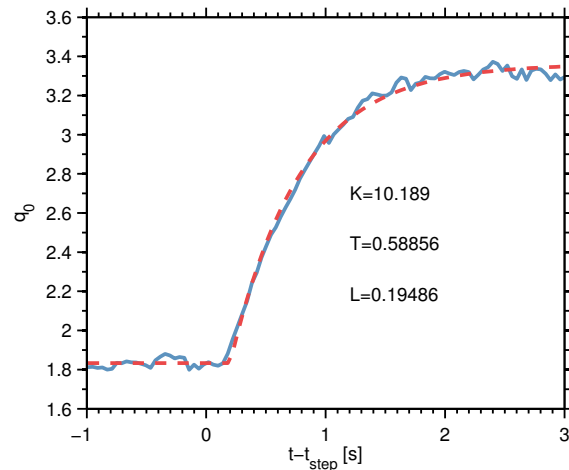


Figure 9: Response of  $q_0$  to a step change in the outer gap.

where  $K$  is the static gain,  $T$  is the time constant, and  $L$  is the dead time. These parameters were identified by studying the response of the output to a step change in the input. A TRANSP simulation of an NSTX-U discharge with  $I_p = 600\text{kA}$  and  $B_T = 1.0\text{T}$  was done in which the outer-gap was held fixed at  $0.05\text{m}$  until a steady value of  $q_0$  was reached, at which point the outer gap was stepped to  $0.20\text{m}$ . During the simulation, the electron particle inventory was fixed at  $5.05 \times 10^{20}$  electrons and the  $\beta_N$  controller regulated the plasma around  $\beta_N = 2.7$ . A curve fitting procedure was used to determine the optimal FOPDT model parameters to match this step response. The step response is compared with the identified model in Figure 9, showing good agreement. The effect of the change in outer gap size on other parameters is depicted in Figure 8. In 8a, it can be seen that the safety factor profile is increased as a result of the beam current drive moving off axis (Figure 8b) and the increase in bootstrap current (Figure 8c). As seen in Figure 8d, the  $\beta_N$  controller successfully kept  $\beta_N$  near its target value. The Greenwald fraction dropped slightly due to the reduction in plasma minor radius. This reduction is shown in Figure 8f along with the increase in elongation (which contributes to the increased bootstrap current) and the decrease in volume. Though not shown, the density increased due to the decrease in plasma volume (recall that the electron inventory was held fixed). The increase in beam current drive efficiency and bootstrap current led to an increase in the non-inductive fraction, as seen in Figure 8e.

The FOPDT model enables the design parameters of the feedback controller to be tuned using the Zeigler-Nichols PID tuning method, a well-known heuristic design algorithm for selecting the gains based on the parameters of the FOPDT model [58], which has been used previously for NSTX control development in [24]. The gains are provided in Table 1. It was found that a PI controller ( $K_D = 0$ ) was sufficient to achieve good performance in this case (the parameters were modified from this starting point empirically to improve the system performance based on the results of Simulink simulations).

Controller type	$K_P$	$K_I$	$K_D$
P	$\frac{1}{K} \frac{T}{L}$	—	—
PI	$\frac{0.9}{K} \frac{T}{L}$	$\frac{K_P}{3.33L}$	—
PID	$\frac{1.2}{K} \frac{T}{L}$	$\frac{K_P}{2.0L}$	$K_P 0.5L$

Table 1: Ziegler and Nichols PID controller gains for FOPDT systems.

A closed loop TRANSP simulation of the two-loop controller was performed using the same simulation parameters as those used for the model identification. The controller was activated at 1s and given a time-varying target that started at  $q_0 = 1.6$  between  $t = 1$ s and 4s, then stepped to  $q_0 = 3.0$  from 4s to the end of the simulation.

Time-dependent results of the closed loop simulation are shown in Figure 10. In Figure 10(a) and (b) the successful tracking of the time-varying targets for  $q_0$  and  $\beta_N$  is evident. The response of  $q_0$  is much faster than the open loop equilibration time, and neither  $q_0$  or  $\beta_N$  exhibit significant overshoot or oscillations (other than those caused by numerical noise). One exception to this is the response of  $q_0$  to the step change in target at  $t = 4.0$ s. The response to this target change was slower than the others due to the saturation of the outer-gap at its maximum allowed value, as can be seen in Figure 10(d). For the rest of the simulation, the outer-gap request did not saturate, although it settled at a value very close to the limit after the step change in the target at  $t = 7.0$ s. The beam-driven, bootstrap, and non-inductive current fractions are compared in Figure 10(c). Each of the quantities increased as the operating points were changed. Though the quantities have complex nonlinear dependence on many plasma parameters, the increase in bootstrap current fraction is likely due primarily to the increase in elongation associated with the larger outer-gap requested after  $t = 4.0$ s, while the increase in beam-driven fraction is due primarily to the increase in NBI power required to track the  $\beta_N$  target after  $t = 4.0$ s and again after  $t = 7.0$ s, as shown in Figure 10(e). Finally, the density, shown in Figure 10(f), increased as the outer-gap-size was increased and the plasma volume decreased, since the particle inventory was held fixed during the simulation.

Profiles at the end of each target step are compared in Figure 11. The first operating point had a low  $q_0$  and was very slightly reverse-shear, due to low bootstrap current and beam-driven current peaked on-axis. At the second operating point, the bootstrap current increased significantly while the beam-driven current decreased on-axis and increased outside of  $\hat{\rho} = 0.25$ . This resulted in a much higher  $q_0$ , and a more reverse-shear safety factor profile. For the third operating point, the beam-driven-current outside of  $\hat{\rho} = 0.35$  matched closely with that of the second operating point, while the on-axis current drive as increased, even above that of the first operating point. The bootstrap current increased slightly over the second operating point level. The net result was an

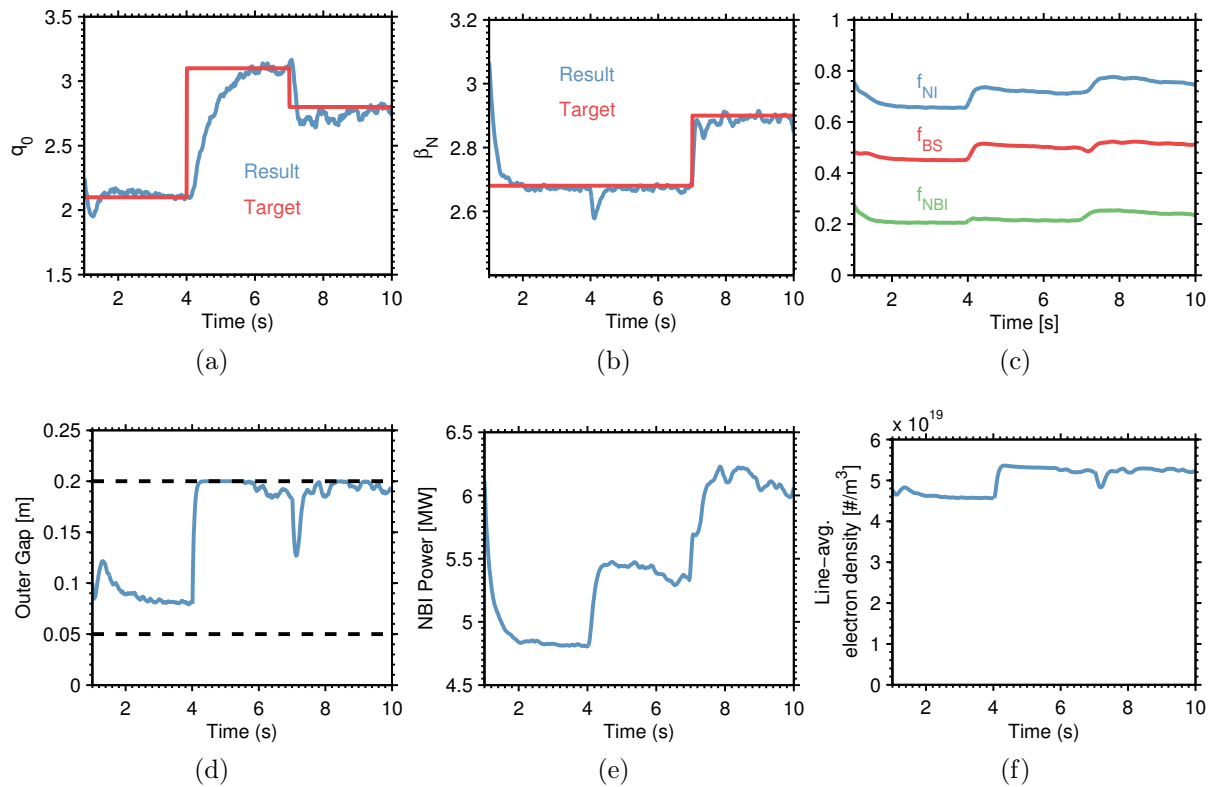


Figure 10: Results of closed loop simulation of the two-loop control scheme: (a)  $q_0$  result compared to target, (b)  $\beta_N$  compared to target, (c) non-inductive current fractions, (d) outer gap, (e) injected power, and (f) electron density.

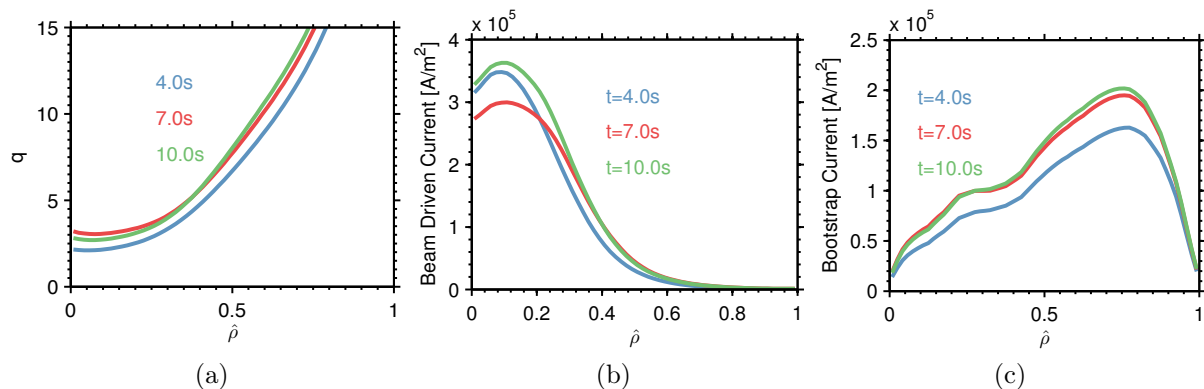


Figure 11: Results of closed loop simulation of the two-loop control scheme: (a)  $q$  profiles, (b) beam driven current profiles, and (c) bootstrap current profiles.

decrease in  $q_0$  and a flatter safety factor profile. The coil current needed to produce the request plasma boundary shapes are shown in Figure 12. The currents are at reasonable levels and the time-evolutions appear to be physically achievable, implying the proposed control approach should be experimentally feasible.

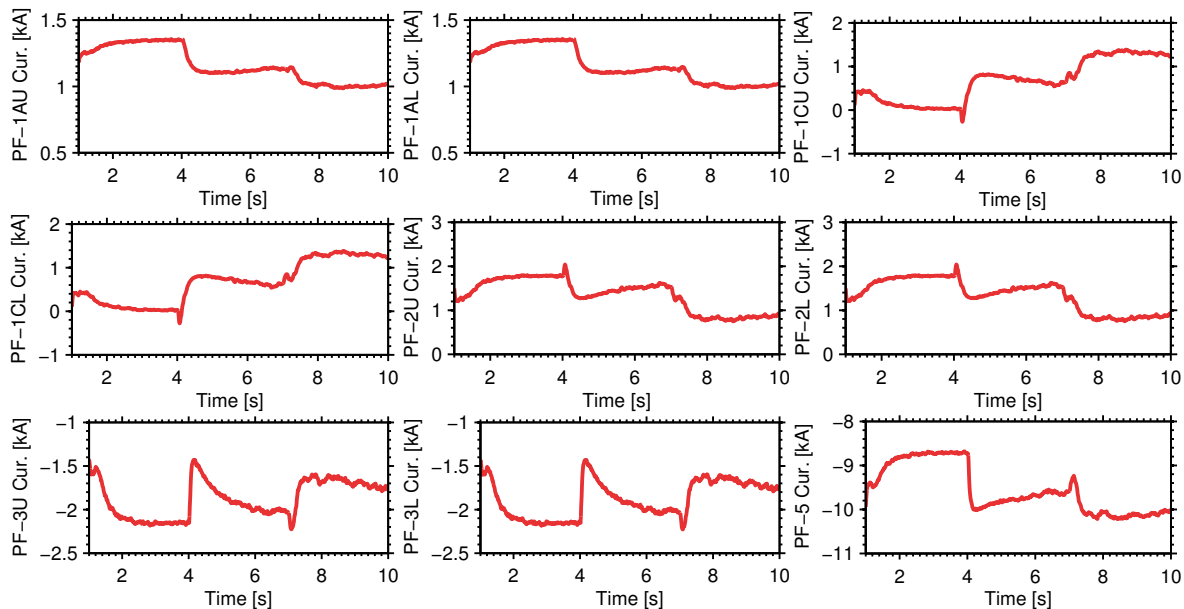


Figure 12: Poloidal field coil currents during closed loop simulation of the two-loop control scheme.

### 4.3. Discussion

From the simulation results shown here, good performance was obtained using both the MIMO optimal controller and two loop control design. From the perspective of an operator, this is desirable, as it indicates the two loop structure, with a small number of free parameters that can be adjusted intuitively between shots, may work well in experiments. However, the optimal design provides a more systematic algorithm for designing a stabilizing controller, is well suited to handling systems with strong cross-coupling, and can be easily extended to include additional controlled variables and actuators. As scenarios that exhibit stronger coupling are explored, or as additional actuators and controlled outputs are considered, the tuning of separate PID loops will become more difficult, while the MIMO control design approach will still be appropriate.

## 5. Conclusion

A novel approach to controlling  $q_0$  and  $\beta_N$  in NSTX-U, in which the outer-midplane wall gap and total beam power serve as manipulated variables, has been proposed. TRANSP simulations of the control schemes show promising results and motivate future experimental implementation. In future work, manipulation of the outer-gap will be integrated into a more complex current profile control scheme that includes modulation of the individual beam powers, plasma density, and loop voltage, to control several points of the safety factor profile simultaneously. The effect of the control scheme on plasma stability and controllability will also be studied in future research, as modifying the outer gap will vary coupling to the passive plates.

As part of this work, a flexible framework for performing feedback control design and simulation in the TRANSP has been developed. This framework will aid in the creation of advanced control algorithms by providing a means for conducting system identification simulations and high-fidelity tests of proposed algorithms prior to experimental implementation and testing. In future work, the framework will be extended to include additional actuators and ‘measurements’ in order to test many of the advanced control algorithms under development for NSTX-U, including plasma boundary shape controllers and profile (safety factor, rotation, etc.) controllers. The framework is also planned to be used for studies of other machines, including DIII-D, ITER, and FNSF (Fusion Nuclear Science Facility).

## Acknowledgements

This research was supported in part by an appointment to the U.S. Department of Energy Fusion Energy Postdoctoral Research Program administered by the Oak Ridge Institute for Science and Education.

## References

- [1] MENARD, J., GERHARDT, S., BELL, M., et al., *Nuclear Fusion* **52** (2012) 083015.
- [2] ONO, M., KAYE, S., PENG, Y.-K., et al., *Nuclear Fusion* **40** (2000) 557.
- [3] SYKES, A., AKERS, R., APPEL, L., et al., *Nuclear Fusion* **41** (2001) 1423.
- [4] GOLDSTON, R., MENARD, J., ALLAIN, J., et al., An Experiment to Tame the Plasma Material Interface FT/P3-12, in *Proc. 22nd Int. Conf. on Fusion Energy*, Geneva, Switzerland, 2008, IAEA.
- [5] STAMBAUGH, R. D., CHAN, V. S., WONG, C. P. C., et al., Candidates for a Fusion Nuclear Science Facility ( FDF and ST-CTF ) P2.110, in *37th EPS Conf. on Plasma Physics*, volume 51, Dublin, Ireland, 2010.
- [6] MENARD, J., BROMBERG, L., BROWN, T., et al., *Nuclear Fusion* **51** (2011) 103014.
- [7] KAYE, S., BELL, M., BELL, R., et al., *Nuclear Fusion* **46** (2006) 848.
- [8] KAYE, S., BELL, R., GATES, D., et al., *Physical Review Letters* **98** (2007) 175002.
- [9] KAYE, S., LEVINTON, F., STUTMAN, D., et al., *Nuclear Fusion* **47** (2007) 499.
- [10] VALOVIC, M., AKERS, R., DE BOCK, M., et al., *Nuclear Fusion* **51** (2011) 073045.
- [11] FREDRICKSON, E. D., BELL, R. E., DARROW, D. S., et al., *Physics of Plasmas* **13** (2006) 056109.
- [12] GRYAZNEVICH, M., SHARAPOV, S., LILLEY, M., et al., *Nuclear Fusion* **48** (2008) 084003.
- [13] PODESTA, M., HEIDBRINK, W. W., LIU, D., et al., *Physics of Plasmas* **16** (2009) 056104.
- [14] FREDRICKSON, E. D., CROCKER, N. A., BELL, R. E., et al., *Physics of Plasmas* **16** (2009) 122505.
- [15] GATES, D., MENARD, J., MAINGI, R., et al., *Nuclear Fusion* **47** (2007) 1376.
- [16] MENARD, J., BELL, M., BELL, R., et al., *Nuclear Fusion* **47** (2007) S645.
- [17] GATES, D., AHN, J., ALLAIN, J., et al., *Nuclear Fusion* **49** (2009) 104016.
- [18] GERHARDT, S., GATES, D., KAYE, S., et al., *Nuclear Fusion* **51** (2011) 073031.
- [19] BUTTERY, R., AKERS, R., ARENDS, E., et al., *Nuclear Fusion* **44** (2004) 1027.
- [20] CHAPMAN, I., COOPER, W., GRAVES, J., et al., *Nuclear Fusion* **51** (2011) 073040.
- [21] ERICKSON, K., GATES, D., GERHARDT, S., et al., *Fusion Engineering and Design* **89** (2014) 853.
- [22] GATES, D., FERRON, J., BELL, M., et al., *Nuclear Fusion* **46** (2006) 17.

- [23] GERHARDT, S., KOLEMEN, E., LAWSON, J., et al., *Fusion Science and Technology* **61** (2010) 11.
- [24] KOLEMEN, E., GATES, D., ROWLEY, C., et al., *Nuclear Fusion* **50** (2010) 105010.
- [25] KOLEMEN, E., GATES, D., GERHARDT, S., et al., *Nuclear Fusion* **51** (2011) 113024.
- [26] KOLEMEN, E., ELLIS, R., LAHAYE, R., et al., *Fusion Engineering and Design* **88** (2013) 2757.
- [27] OU, Y., LUCE, T., SCHUSTER, E., et al., *Fusion Engineering and Design* **82** (2007) 1153.
- [28] BARTON, J. E., BOYER, M. D., SHI, W., et al., *Nuclear Fusion* **52** (2012) 123018.
- [29] BOYER, M. D., BARTON, J., SCHUSTER, E., et al., *Plasma Physics and Controlled Fusion* **55** (2013) 105007.
- [30] BOYER, M. D., BARTON, J., SCHUSTER, E., et al., *IEEE Transactions on Control Systems Technology* **22** (2014) 1725.
- [31] MOREAU, D., MAZON, D., ARIOLA, M., et al., *Nuclear Fusion* **48** (2008) 106001.
- [32] MOREAU, D., MAZON, D., WALKER, M., et al., *Nuclear Fusion* **51** (2011) 063009.
- [33] TURNBULL, A. D., LIN-LIU, Y. R., MILLER, R. L., TAYLOR, T. S., and TODD, T. N., *Physics of Plasmas* **6** (1999) 1113.
- [34] HOLCOMB, C. T., FERRON, J. R., LUCE, T. C., et al., *Physics of Plasmas* **16** (2009) 056116.
- [35] GERHARDT, S., ANDRE, R., and MENARD, J., *Nuclear Fusion* **52** (2012) 083020.
- [36] MENARD, J., BELL, R., FREDRICKSON, E., et al., *Nuclear Fusion* **45** (2005) 539.
- [37] MENARD, J., BELL, R., GATES, D., et al., *Physical Review Letters* **97** (2006) 095002.
- [38] CHAPMAN, I., HUA, M.-D., PINCHES, S., et al., *Nuclear Fusion* **50** (2010) 045007.
- [39] BRESLAU, J., CHANCE, M., CHEN, J., et al., *Nuclear Fusion* **51** (2011) 063027.
- [40] GERHARDT, S., BRENNAN, D., BUTTERY, R., et al., *Nuclear Fusion* **49** (2009) 032003.
- [41] HAWRYLUK, R., An Empirical Approach To Tokamak Transport, in COPPI, B., editor, *Physics of Plasmas Close to Thermonuclear Conditions: Proceedings of the Course Held in Varenna, Italy, 27 August-8 September 1979*, volume 1, pp. 19–46, Varenna, Italy, 1981, Elsevier Ltd.
- [42] BUDNY, R., *Nuclear Fusion* **34** (1994) 1247.
- [43] TRANSP Homepage, 2014.
- [44] PANKIN, A., MCCUNE, D., ANDRE, R., BATEMAN, G., and KRITZ, A., *Computer Physics Communications* **159** (2004) 157.
- [45] HUANG, J. and MENARD, J., Development of an auto-convergent free-boundary axisymmetric equilibrium solver, in *American Physical Society, 47th Annual DPP Meeting*, Denver, Colorado, 2005, American Physical Society.
- [46] ANDRE, R., TRANSP / PTRANSF Isolver Free Boundary Equilibrium Solver, in *American Physical Society, 54th Annual DPP Meeting*, Providence, Rhode Island, 2012, American Physical Society.
- [47] ZARNSTORFF, M. C., MCGUIRE, K., BELL, M. G., et al., *Physics of Fluids B: Plasma Physics* **2** (1990) 1852.
- [48] SAUTER, O., ANGIONI, C., and LIN-LIU, Y. R., *Physics of Plasmas* **6** (1999) 2834.
- [49] LIN-LIU, Y. R. and HINTON, F. L., *Physics of Plasmas* **4** (1997) 4179.
- [50] STAEBLER, G., COLYER, G., KAYE, S., KINSEY, J., and WALTZ, R., Testing the Trapped Gyro-Landau Fluid Transport Model with Data from Tokamaks and Spherical Tori, in *Proc. 22nd IAEA Fusion Energy Conference*, Geneva, Switzerland, 2008, IAEA.
- [51] CHANG, C. S., *Physics of Fluids* **25** (1982) 1493.
- [52] GREENWALD, M., TERRY, J., WOLFE, S., et al., *Nuclear Fusion* **28** (1988) 2199.
- [53] GREENWALD, M., *Nuclear Fusion* **44** (2002) R27.
- [54] ITER Physics Experts Groups, *Nuclear Fusion* **39** (1999) 2175.
- [55] LJUNG, L., *System Identification: Theory for the User*, Prentice Hall, Upper Saddle River, N.J., 2nd edition, 1999.
- [56] MATLAB and System Identification Toolbox Release 2013a.
- [57] FRANKLIN, G., POWELL, J., and WORKMAN, M., *Digital Control of Dynamic Systems*, Addison-Wiley, second edition, 1990.

- [58] XUE, D., CHEN, Y., and ATHERTON, D., *Linear Feedback Control: Analysis and Design with MATLAB (Advances in Design and Control)*, Society for Industrial and Applied Mathematics, Philadelphia, PA, 2008.

---

# Princeton Plasma Physics Laboratory Office of Reports and Publications

Managed by  
Princeton University

under contract with the  
U.S. Department of Energy  
(DE-AC02-09CH11466)

---

P.O. Box 451, Princeton, NJ 08543  
Phone: 609-243-2245  
Fax: 609-243-2751

E-mail: [publications@pppl.gov](mailto:publications@pppl.gov)

Website: <http://www.pppl.gov>